Thermally induced crystal-to-crystal transformations accompanied by changes in the magnetic properties of a Cu^{II}-*p*-hydroquinonate polymer†

Ngoc Hien Phan,[a] Ivan Halasz,[b] Ingo Opahle,[c] Edith Alig,[a] Lothar Fink,[a] Jan W. Bats,[d] Pham Thanh Cong,[e] Hans-Wolfram Lerner,[a] Biprajit Sarkar,[f] Bernd Wolf,[e] Harald O. Jeschke,[c] Michael Lang,*[e] Roser Valentí,*[c] Robert Dinnebier*[b] and Matthias Wagner*[a]

In the Cu^{II}-*p*-hydroquinonate coordination polymer **1**, the major pathway for antiferromagnetic exchange coupling runs along the hydroquinonate linker. Upon heating, **1** looses its supporting DMF ligands in a two-step sequence; the antiferromagnetic Cu^{II}–Cu^{II} interaction in the final product **3** is now mediated by two bridging oxygen atoms which results in an increase of the *J* value by two orders of magnitude.

The physical properties of linear spin chains and two-dimensional spin networks differ substantially from the magnetic behavior of materials in which spins are three-dimensionally coupled.[1–4] For studying the quantum many-body effects in these different regimes, crystalline networks of paramagnetic dinuclear complexes which provide closely spaced pairs of $S = \frac{1}{2}$ spins coupled antiferromagnetically have been particularly useful. Of special interest has been the use of molecular-based dimers with a moderate strength of the intra-dimer exchange coupling ($J_{dimer} \approx 10$ K k_B). When such systems are exposed to a magnetic field strong enough to close the spin gap, a gas of bosonic excitations is generated,[5] leading to remarkable physical phenomena like Bose–Einstein condensation[6] or Luttinger-liquid behavior.[7]

It has been shown that modified *p*-hydroquinonate ligands can mediate spin–spin coupling of the desired magnitude.[8–11] Supported by this background, our group is currently studying the Cu^{II} ($S = \frac{1}{2}$)

coordination polymer **1** (Scheme 1).[12] The compound readily crystallizes from a mixture of dimethylformamide (DMF) and diethyl ether (Et$_2$O).[12]

So far, the main interest in this material has arisen due to the fact that it undergoes a magnetic field-induced phase transition at low temperatures[13] showing a 2D signature. We now want to report on the rich solid-state chemistry of **1**, which provides an excellent setscrew for subtle manipulations of the bulk aggregates thereby

[a]Institut für Anorganische Chemie, Goethe-Universität Frankfurt, Max-von-Laue-Str. 7, D-60438 Frankfurt (Main), Germany. E-mail: Matthias.Wagner@chemie.uni-frankfurt.de; Fax: +49 69 798 29260
[b]Max-Planck-Institut für Festkörperforschung, Heisenbergstr. 1, D-70569 Stuttgart, Germany. E-mail: R.Dinnebier@fkf.mpg.de; Fax: +49 711 689 1502
[c]Institut für Theoretische Physik, Goethe-Universität Frankfurt, Max-von-Laue-Str. 1, D-60438 Frankfurt (Main), Germany. E-mail: valenti@itp.uni-frankfurt.de; Fax: +49 69 798 47832
[d]Institut für Organische Chemie, Goethe-Universität Frankfurt, Max-von-Laue-Str. 7, D-60438 Frankfurt (Main), Germany
[e]Physikalisches Institut, Goethe-Universität Frankfurt, Max-von-Laue-Str. 1, D-60438 Frankfurt (Main), Germany. E-mail: michael.lang@physik.uni-frankfurt.de; Fax: +49 69 798 47250
[f]Institut für Anorganische Chemie, Universität Stuttgart, Pfaffenwaldring 55, D-70569 Stuttgart, Germany

Scheme 1 Synthesis of **2** and **3** by thermal treatment of **1**.

leading to important insights into structure–magnetic property relationships.

The starting point of all investigations reported here was the observation that **1** readily loses its DMF ligands upon thermal treatment and that a high degree of crystallinity is preserved in the DMF-free product. Crystal-to-crystal transitions of molecular materials are among the most fascinating subjects of solid-state science. It is well-known that aging or a temperature rise can lead to the reversible removal of guest molecules present in the crystal lattice of a highly rigid apohost framework. Moreover, various molecular materials undergo structural phase transitions as a function of temperature, and sometimes the original structure can be reformed on returning to the initial temperature. In contrast, only scattered examples have been described of extensive bond cleavage or formation in a bulk material without breakdown of the crystal lattice.[14] In the context of this paper, the few known crystal-to-crystal transformations involving dimensionality changes of coordination complexes and generating a tunable magnetic system are particularly noteworthy.[15] Such tunable molecular magnets, whose structures and properties are sensitive to external stimuli (*e.g.* heat, light, pressure, guest molecules), are attracting increasing attention because of potential applications as switches or sensors.[16] We will show that compound **1** represents a novel system in this context, which, by successive loss of DMF ligands, undergoes a two-step transformation from a single crystal to a single crystal to a microcrystalline solid. The accompanying changes in the material's chemical composition and structure result in an alteration of the magnitude of the major coupling constant (step 1) and in a switch in the major coupling pathway together with a fundamental change in the bulk magnetic properties (step 2).

Key thermodynamic data on the DMF liberation reaction of **1** were obtained by differential thermal analysis (DTA) and thermogravimetric analysis (TGA). A crystalline sample of **1** was heated in an alumina crucible to a temperature of 200 °C (rate: 5 °C min^{-1}; N$_2$ atmosphere). A 12% weight loss, accompanied by an endotherm in the DTA curve (*cf.* ESI†), is observable in the temperature interval of 70–120 °C and corresponds to the loss of two DMF molecules per repeat unit (*cf.* **2**; Scheme 1). Two more equivalents of DMF are liberated in a second step with an onset temperature of approximately 160 °C (*cf.* **3**; Scheme 1).

Based on these analytical measurements, we then placed a particularly well-grown single crystal of **1** into the DTA/TGA crucible, slowly increased the temperature to 85 °C and maintained this temperature until the weight loss had come to an end. After cooling to rt, the specimen (**2**), which turned out to be still single-crystalline, was subjected to X-ray crystallography. Similar experiments employing higher temperatures showed that the liberation of the second two equivalents of DMF cannot be carried out as single crystal-to-single crystal transition. To obtain structural information on the DMF-free species **3**, we therefore used a gently ground sample of **1**, heated it in a borosilicate capillary to a final temperature of 220 °C and solved the structure of the resulting material on the basis of high-resolution X-ray powder diffraction data.

The X-ray crystal structure analysis of **1** has already been described by our group.[12] The compound crystallizes from Et$_2$O/DMF as red-brown needles. Compound **1** is a coordination polymer in the solid state (see below); the centrosymmetric repeat unit consists of a dinuclear, dicationic *p*-hydroquinonate-bridged Cu^{II} complex (Fig. 1, top).
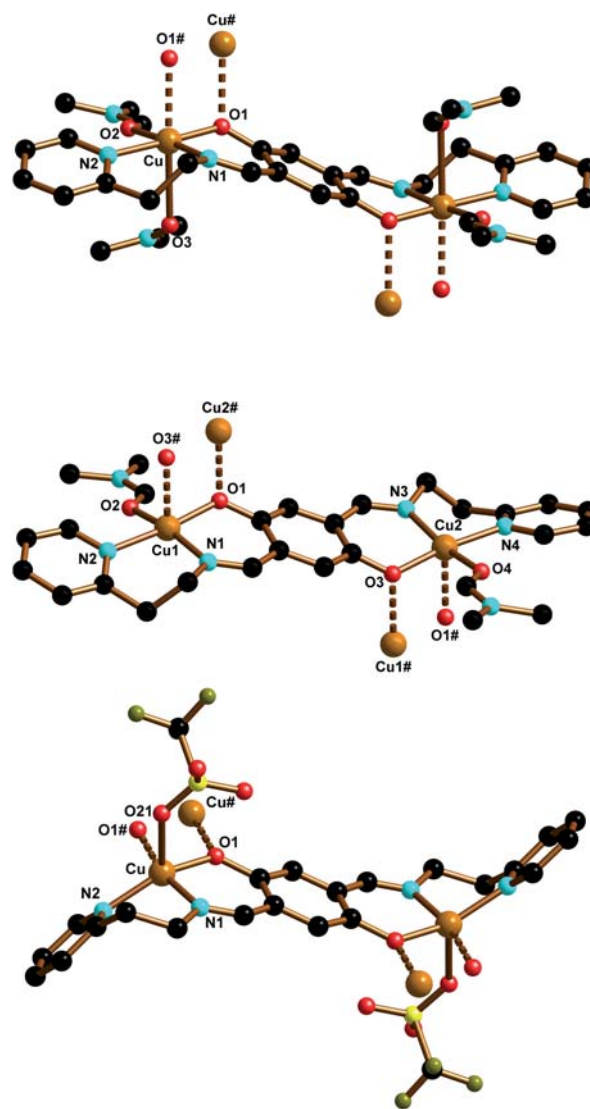
Fig. 1 Molecular structures and numbering schemes of the repeat units of **1** (top), **2** (middle), and **3** (bottom); H-atoms omitted for clarity. Selected bond lengths [Å] and bond angles [°]: **1**: Cu–O(1) 1.930(1), Cu–O(2) 2.001(1), Cu–O(3) 2.565(2), Cu–N(1) 1.965(2), Cu–N(2) 2.075(2), Cu–O(1#) 2.434(1); O(1)–Cu–N(1) 90.9(1), O(1)–Cu–N(2) 175.6(1), N(1)–Cu–N(2) 93.5(1), O(1)–Cu–O(1#) 83.4(1), Cu–O(1)–Cu(1#) 96.6(1). Symmetry transformation used to generate equivalent atoms: #: −x, −y + 1, −z. **2**: Cu(1)–O(1) 1.931(6), Cu(1)–O(2) 1.985(8), Cu(1)–N(1) 1.984(8), Cu(1)–N(2) 2.051(8), Cu(1)–O(3#) 2.343(7), Cu(2)–O(3) 1.920(7), Cu(2)–O(4) 2.006(7), Cu(2)–N(3) 1.956(9), Cu(2)–N(4) 2.063(8), Cu(2#)–O(1) 2.338(7); O(1)–Cu(1)–N(1) 91.1(3), O(1)–Cu(1)–N(2) 173.5(3), N(1)–Cu(1)–N(2) 95.2(3), O(1)–Cu(1)–O(3#) 82.5(3), O(3)–Cu(2)–N(3) 92.1(3), O(3)–Cu(2)–N(4) 173.0(3), N(3)–Cu(2)–N(4) 94.0(3), O(1)–Cu(2#)–O(3#) 82.9(3), Cu(1)–O(1)–Cu(2#) 97.2(2), Cu(1)–O(3#)–Cu(2#) 97.3(3). Symmetry transformation used to generate equivalent atoms: #: *x* + 1, *y*, *z*. **3**: Cu–O(1) 1.921(2), Cu–O(21) 2.332(5), Cu–N(1) 1.940(5), Cu–N(2) 2.020(6), Cu–O(1#) 1.908(2); O(1)–Cu–N(1) 92.7(2), O(1)–Cu–N(2) 151.5(1), N(1)–Cu–N(2) 94.3(2), O(1)–Cu–O(21) 102.2(2), O(1)–Cu–O(1#) 75.4(3), Cu–O(1)–Cu(1#) 104.6(1). Symmetry transformation used to generate equivalent atoms: #: −x, −y, −z.

Each Cu^{II} ion of **1** lies at the center of a Jahn–Teller distorted octahedron consisting of the meridionally coordinating hydroquinonate ligand, two DMF molecules and, in an apical position, the

oxygen atom of a neighboring hydroquinone fragment. The Cu–O(3) bond to the DMF molecule occupying the second apical position is longer by 0.564(2) Å than the Cu–O(2) bond to the equatorially coordinating DMF ligand. As expected from this observation, the apical DMF molecules are the ones that are liberated during the transition of **1 → 2**. Compound **2** also forms coordination polymers in the crystal lattice, the repeat unit, however, is no longer centrosymmetric (Fig. 1, middle; most differences between analogous bond lengths and angles about Cu(1) and Cu(2) fall within the 3σ error margins). Compared to **1**, the loss of the two apical DMF ligands does not result in systematic changes of key structure parameters of the dinuclear entity. We therefore conclude that these ligands are too weakly bound to have a significant impact on the coordination environment of the repeat unit of compound **2**. Upon going from **2** to **3**, loss of the two remaining DMF ligands is observed (Fig. 1, bottom). Nevertheless, the material still preserves a polymeric nature, even though significant differences are obvious in the way the individual repeat units are connected to each other (see below). Remarkably, the triflate ions, which do not form close contacts to the Cu^{II} ions in **1** and **2**, are now coordinated to the metal centers (Cu–O(21) = 2.332(5) Å), thereby completing a distorted square-pyramidal coordination environment ($\tau_5 = 0.24^{17}$). We further note a contraction of the Cu–N(1) and Cu–N(2) bonds by 0.030 Å and 0.038 Å, respectively, compared to the corresponding average values in **2**.

In coordination polymer **1**, the individual repeat units are connected by bridging hydroquinonate oxygen atoms which occupy the second apical position of each ligand octahedron (*cf.* Scheme 1). The best planes through the resulting four-membered Cu$_2$O$_2$ rings are almost perpendicular to the equatorial planes of the Cu complexes (dihedral angle: CuO(1)Cu#O(1#)//CuO(1)O(2)N(1)N(2) = 86.0°); the inter-dimer Cu–O(1#) bond (2.434(1) Å) is longer by 0.504(1) Å than the intra-dimer Cu–O(1) bond (1.930(1) Å).

The connectivity pattern along the polymer backbone of **2** (Scheme 1) is qualitatively similar to that of **1** (dihedral angles: Cu(1)O(1)-Cu(2#)O(3#)//Cu(1)O(1)O(2)N(1)N(2) = 89.0°, Cu(1#)O(1#)-Cu(2)O(3)//Cu(2)O(3)O(4)N(3)N(4) = 85.4°). The major difference lies in the inter-dimer Cu–O contacts, which are approximately 0.09 Å shorter than those of **1** (Cu(1)–O(3#) = 2.343(7) Å, Cu(2#)–O(1) = 2.338(7) Å).

An inspection of the way the polymer strands are arranged in the crystal lattice reveals further differences between **1** and **2** (Fig. 2): in **1**, all Cu ions are located on one straight line and all Cu# atoms on a second straight line. These lines are parallel to each other and to the crystallographic *a* axis, which corresponds to the needle axis of the crystal. In **2**, the Cu(1) ions on one hand and the Cu(2) ions on the other are arranged along parallel straight lines orthogonal to a twofold screw axis. As a result of this newly introduced symmetry element, the *p*-hydroquinonate bridges of two neighboring polymer strands are no longer coplanar, but include dihedral angles of 61.7°.

The most striking variation between the connectivity patterns of **1/2** *versus* **3** lies in the fact that the Cu$_2$O$_2$ rings of **3** are no longer orthogonal to the basal plane of the Cu complex, but almost coplanar to it (CuO(1)Cu#O(1#)//CuO(1)N(1) = 7.6°). In further contrast to **2**, the polymer main axes defined by the Cu atoms are now parallel to the twofold screw axis and, similar to **1**, all hydroquinone bridges are coplanar to each other. The inter-dimer bonds in **3** amount to Cu–O(1#) = 1.908(2) Å, which is shorter by about 0.43 Å than the related bonds in **2** and almost equal to the intra-dimer bond of **3**
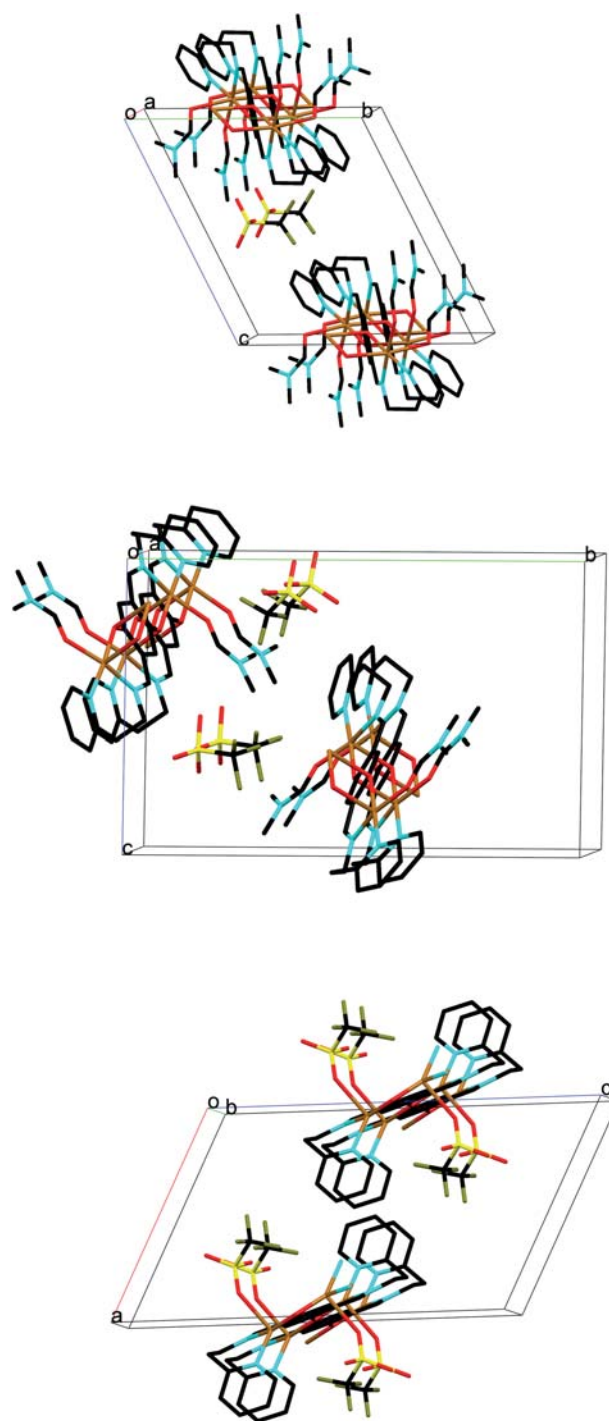
Fig. 2 Crystal packing diagrams of compounds **1**, **2**, and **3**. View along the polymer main chains; in the diagrams of **1** and **2**, several triflate ions have been omitted for clarity. For atom labelling the same colour code as in Fig. 1 has been used.

(Cu–O(1) = 1.921(2) Å). With regard to the Cu–O(1)–Cu# bond angle, which is of prime importance for the magnetic properties of the material, the best Rietveld fit was obtained for a value of 104.6(1)°.

Fig. 3 shows the molar susceptibilities ($\chi_{mol}(T)$) of **1**, **2**, and **3** on a logarithmic temperature scale (*note*: the magnetic behavior of **1** is partially restored when **3** is exposed to an atmosphere of DMF).
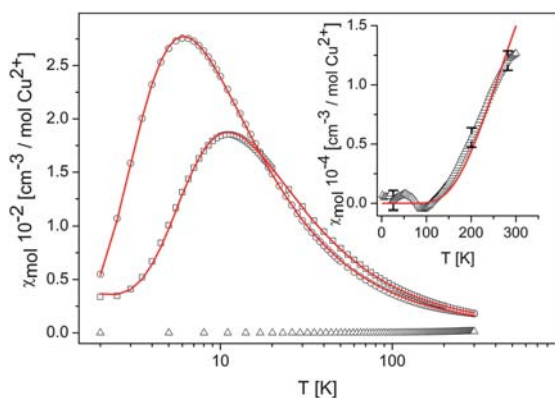
Fig. 3 Molar magnetic susceptibility $\chi_{mol}(T)$ of **1** (open circles), **2** (open squares) and **3** (open triangles) after subtraction of the background contribution. The solid lines are least-squares fits to the experimental data based on isolated-dimer models. Inset: blow-up of $\chi_{mol}(T)$ of **3** (open triangles) on a linear temperature scale together with a fit based on an isolated-dimer model (solid red lines).

The data were corrected for magnetic background contributions as described in the ESI†. The magnetic properties of **1** and **2** are similar in showing a broad maximum of the $\chi_{mol}(T)$ curve around 10 K followed by a rapid decrease in $\chi_{mol}(T)$ with decreasing temperature. This indicates the opening of a small spin gap and the formation of a spin-singlet ($S = 0$) ground state as expected for dominant intra-dimer interactions. Fits based on an isolated-dimer model[18] with an antiferromagnetic intra-dimer coupling constant of $J = (9.8 \pm 0.1)$ K k_B (**1**) and $J = (18.2 \pm 0.1)$ K k_B (**2**) provide an excellent description of the data. For **3** the spin gap appears to be greatly enhanced as the system is essentially non-magnetic over the whole temperature range investigated (*cf.* the main panel of Fig. 3). However, as the data in the inset of Fig. 3 clearly show, $\chi_{mol}(T)$ of **3** exhibits a significant increase towards higher temperatures. Despite the small size of the magnetic signal (implying noticeable error bars as indicated in the inset), the data can be well described by the isolated-dimer model with an antiferromagnetic coupling constant $J = (1050 \pm 50)$ K k_B.

We emphasize that the major coupling pathways are distinctly different in **1/2** on the one hand and **3** on the other. In **1**, the spin–spin coupling is mainly mediated by the hydroquinonate bridge; the inter-dimer coupling *via* the Cu#–O1#–Cu bonds is one order of magnitude smaller.[12] In **3**, however, this latter pathway becomes dominant, because the O1#–Cu vector is no longer orthogonal to the magnetic Cu $d(x^2 - y^2)$ orbital, but lies essentially in the same plane.

EPR spectroscopy on **1**, **2**, and **3** is in full accord with the magnetic susceptibility measurements in that **1** and **2** show the distinct aniso-tropic signals of paramagnetic Cu^{II} complexes, whereas **3** is EPR silent (*cf.* ESI†).

To gain further insight into the electronic structure of **3** and to corroborate our interpretation of its magnetic susceptibility data, the experiments were augmented by DFT calculations. Fig. 4 shows the nonmagnetic LDA density of states (DOS) and band structure of **3** along selected symmetry lines in the Brillouin zone.

The DOS in the vicinity of the Fermi energy is dominated by Cu(3d) states and O(2p) states with contributions of N(2p) states as well as C(2p) derived states. The Cu(3d) states form narrow bands with a width of about 0.1–0.2 eV in the energy region between −2.5 eV and 0.5 eV. The valence bands are separated from the conduction
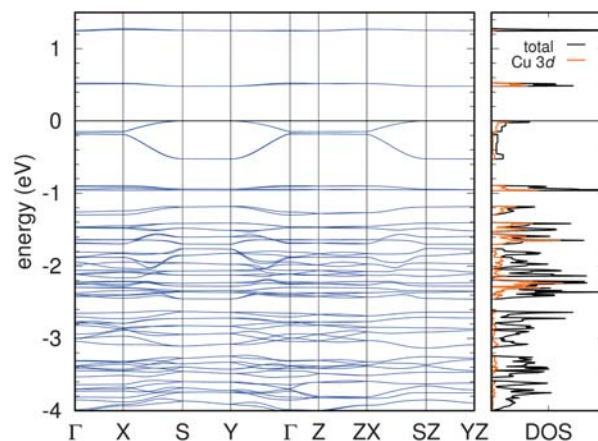
Fig. 4 Nonmagnetic LDA density of states and band structure in the vicinity of the Fermi energy along selected high symmetry lines in the Brillouin zone of **3**.

bands by a gap of about 0.5 eV already in the nonmagnetic LDA calculations. The upper valence band and the lower conduction band have mainly Cu(3d) character.

Next, we address the magnetic state of **3**. The ground state is an antiferromagnet with the spins of the nearest neighbor Cu^{II} ions aligned in an anti-parallel fashion. Due to the environment of the Cu^{II} ions and the narrow band width of the Cu(3d) states, a realistic treatment of the magnetic couplings requires to take into account the strong onsite Coulomb correlations. An appropriate method is thus the LSDA + U formalism. The calculated exchange couplings are shown in Table 1, where we used the Slater parameters $F_0 = 6.0$ eV, $F_2 = 8.6$ eV, $F_4 = 5.4$ eV for the parameters of the LSDA + U functional, corresponding to typical values of $U = 6.0$ eV and $J = 1.0$ eV for the Cu(3d) orbitals in this environment.

The calculations show that the major coupling interaction is the one between nearest neighbor Cu^{II} ions (across a bridging O atom) with a huge coupling constant of $J_1 = 77.3$ meV (approx. 900 K k_B; AMF functional) or 125 meV (approx. 1450 K k_B; AL functional). In **3**, the J_1 value is thus more than two orders of magnitude larger than the antiferromagnetic J_2 coupling constant between two Cu^{II} ions across the hydroquinonate bridge (Table 1). This result means that the magnetic degrees of freedom in **3** are frozen in the experimentally accessible temperature range, in agreement with the susceptibility measurements presented above.

In summary, we have shown that subtle structural changes in low-dimensional spin systems can result in serious modifications of their magnetic behavior (*cf.* the doubling of the intra-dimer coupling constant upon going from **1** to **2**). Moreover, the removal of weakly bound supporting ligands can have a dramatic impact on the bulk physical properties of coordination polymers (*cf.* the non-magnetic

Table 1 Calculated exchange constants for **3** using $U = 6$ eV and $J = 1$ eV

	LSDA + U(AMF)	LSDA + U(AL)	Cu–Cu distance/Å
J_1 [meV]/J_1 [K k_B]	77.3/897	125/1451	3.035
J_2 [meV]/J_2 [K k_B]	0.3/3.5	0.5/5.8	8.493

behavior of **3**). We therefore note that an *a posteriori* adjustment of single crystals provides a powerful tool for the preparation of novel spin lattices and thus a viable alternative to classic crystal engineering attempts.

Notes and references

1 O. Kahn, *Molecular Magnetism*, VCH, New York, 1993.
2 J. S. Miller and M. Drillon, *Magnetism: Molecules to Materials I–III*, Wiley-VCH, Weinheim, 2001.
3 N. D. Mermin and H. Wagner, *Phys. Rev. Lett.*, 1966, **17**, 1133.
4 J. M. Kosterlitz and D. J. Thouless, *J. Phys. C: Solid State Phys.*, 1973, **6**, 1181.
5 T. Giamarchi, C. Rüegg and O. Tchernyshyov, *Nat. Phys.*, 2008, **4**, 198.
6 T. Nikuni, M. Oshikawa, A. Oosawa and H. Tanaka, *Phys. Rev. Lett.*, 2000, **84**, 5868.
7 C. Rüegg, K. Kiefer, B. Thielemann, D. F. McMorrow, V. Zapf, B. Normand, M. B. Zvonarev, P. Bouillot, C. Kollath, T. Giamarchi, S. Capponi, D. Poilblanc, D. Biner and K. W. Krämer, *Phys. Rev. Lett.*, 2008, **101**, 247202.
8 R. Dinnebier, H.-W. Lerner, L. Ding, K. Shankland, W. I. F. David, P. W. Stephens and M. Wagner, *Z. Anorg. Allg. Chem.*, 2002, **628**, 310.
9 G. Margraf, T. Kretz, F. Fabrizi de Biani, F. Laschi, S. Losi, P. Zanello, J. W. Bats, B. Wolf, K. Remović-Langer, M. Lang, A. Prokofiev, W. Assmus, H.-W. Lerner and M. Wagner, *Inorg. Chem.*, 2006, **45**, 1277.
10 B. Wolf, S. Zherlitsyn, B. Lüthi, N. Harrison, U. Löw, V. Pashchenko, M. Lang, G. Margraf, H.-W. Lerner, E. Dahlmann, F. Ritter, W. Assmus and M. Wagner, *Phys. Rev. B: Condens. Matter Mater. Phys.*, 2004, **69**, 092403.
11 B. Wolf, A. Brühl, J. Magerkurth, S. Zherlitsyn, V. Pashchenko, B. Brendel, G. Margraf, H.-W. Lerner, M. Wagner, B. Lüthi and M. Lang, *J. Magn. Magn. Mater.*, 2005, **290–291**, 411.
12 T. Kretz, J. W. Bats, S. Losi, B. Wolf, H.-W. Lerner, M. Lang, P. Zanello and M. Wagner, *Dalton Trans.*, 2006, 4914.
13 Y. Tsui, A. Brühl, K. Removic-Langer, V. Pashchenko, B. Wolf, G. Donath, A. Pikul, T. Kretz, H.-W. Lerner, M. Wagner, A. Salguero, T. Saha-Dasgupta, B. Rahaman, R. Valenti and M. Lang, *J. Magn. Magn. Mater.*, 2007, **310**, 1319.
14 (*a*) I. G. Georgiev and L. R. MacGillivray, *Chem. Soc. Rev.*, 2007, **36**, 1239; (*b*) J. J. Vittal, *Coord. Chem. Rev.*, 2007, **251**, 1781; (*c*) S. Kitagawa and R. Matsuda, *Coord. Chem. Rev.*, 2007, **251**, 2490; (*d*) M. Kawano and M. Fujita, *Coord. Chem. Rev.*, 2007, **251**, 2592; (*e*) L. R. MacGillivray, G. S. Papaefstathiou, T. Friščić, T. D. Hamilton, D.-K. Bučar, Q. Chu, D. B. Varshney and I. G. Georgiev, *Acc. Chem. Res.*, 2008, **41**, 280; (*f*) I. Halasz, *Cryst. Growth Des.*, 2010, **10**, 2817.
15 (*a*) D. Riou, O. Roubeau and G. Férey, *Z. Anorg. Allg. Chem.*, 1998, **624**, 1021; (*b*) D. Bradshaw, J. E. Warren and M. J. Rosseinsky, *Science*, 2007, **315**, 977; (*c*) W. Kaneko, M. Ohba and S. Kitagawa, *J. Am. Chem. Soc.*, 2007, **129**, 13706; (*d*) X.-N. Cheng, W.-X. Zhang and X.-M. Chen, *J. Am. Chem. Soc.*, 2007, **129**, 15738; (*e*) Y.-J. Zhang, T. Liu, S. Kanegawa and O. Sato, *J. Am. Chem. Soc.*, 2009, **131**, 7942.
16 O. Sato, J. Tao and Y.-Z. Zhang, *Angew. Chem., Int. Ed.*, 2007, **46**, 2152.
17 For five-coordinate complexes, the geometry index $\tau_5 = (\theta - \phi)/60°$ provides a quantitative measure of whether the ligand sphere more closely approaches a square-pyramidal ($\tau_5 = 0$) or a trigonal-bipyramidal geometry ($\tau_5 = 1$; θ and ϕ are the two largest bond angles and $\theta \geq \phi$): A. W. Addison, T. N. Rao, J. Reedijk, J. van Rijn and G. C. Verschoor, *J. Chem. Soc., Dalton Trans.*, 1984, 1349.
18 B. Bleaney and K. D. Bowers, *Proc. R. Soc. London, Ser. A*, 1952, **214**, 451.